Journal of Heat and Mass Transfer Research

Journal homepage: http://jhmtr.semnan.ac.ir

Semnan University

Effects of Radiation Absorption, Soret and Dufour on Unsteady MHD Mixed Convective Flow past a Vertical Permeable Plate with Slip Condition and Viscous Dissipation

Temjennaro Jamir *, **Hemanta Konwar**

Kohima Science College, Jotsoma, Nagaland 797002, India.

PAPER INFO

Paper history:

Received: 2022-10-18
Revised: 2023-01-28
Accepted: 2023-02-03

Keywords:

Radiation absorption;
Porous medium;
Slip flow;
Soret;
Dufour;
Viscous Dissipation.

ABSTRACT

Objective: The objective of current study is to discuss the effects of the Soret and Dufour with radiation absorption, applied heat source and viscous dissipation on an unsteady MHD mixed convective flow with velocity slip condition across a semi-infinite vertical permeable plate in porous medium. **Method:** A similarity transformation is used to turn the governing partial differential equations with proper boundary conditions into coupled, non-linear ordinary differential equations with variable coefficients. The inbuilt MATLAB solver bvp4c is used to generate numerical solutions. **Findings:** The effects on momentum, thermal and solutal boundary layers for various parametric values are graphically depicted. Skin friction, Nusselt number and Sherwood number are all tabulated and discussed in detail. An improvement in radiation absorption corresponds to enhancement of the heat transfer rate up to 59% while leading to a decline in mass transfer rate around 20%. The momentum, thermal and solutal boundary layers are all found to be boosted when the Soret effect is higher. For higher estimation of slip effect, the skin friction is found to decay around 23%. Also, as more time goes by the thermal and concentration boundary layers are enhanced. **Novelty:** Results obtained in this studied has also been compared and verified with available scientific literature and is found to be in good agreement, which establishes assurance in the numerical results reported in the study.

DOI: 10.22075/jhmtr.2023.28693.1399

1. Introduction

Navier explored a boundary condition of fluid slip at a solid surface such that the solid surface velocity is proportional to the shear stress at the surface in the history of fluid flow via channels, that is $u = h\,\partial u/\partial y$, where the slip coefficient is h and the velocity along the x-axis is u [1]. The flow regime is known as the slip flow regime, and the significance of its consequences in applications such as micro channel and mechanical device lubrication, where a little layer of lubricant is applied to the surfaces to prevent them from rubbing against one another, or when the surfaces are coated with a particular type of coating to lessen friction. Furthermore, in polymer melts, which frequently display tiny wall slip, make the insufficiency of the no-slip criterion abundantly clear. The synchronisation of the velocities and stresses is one of the boundary requirements that must be met at the contact between a porous material and fluid layer.

Beavers and Joseph [2] analysed fluid flow at the boundary between a porous medium and fluid layer in an experimental research and established a slip boundary conditions at the porous interface.

Pal and Talukdar [3] also contributed a numerical analysis on the influence of ohmic heating and magnetic field for a mixed convective fluid flow problem taking into consideration the boundary slip effect. A numerical study of the velocity and thermal wall slip on MHD boundary layer viscous flow over a non-linearly-stretching sheet was also considered by Ramya et al. [4].

*Corresponding Author: Temjennaro Jamir
Email: temjennaro@kscj.ac.in

Numerous research has also focused on issues with heat and mass transfer in radiative convective flow. Because of its far-reaching contributions in the realm of engineering, such as its use in MHD bearings and MHD pumps. Surface heat transfer is significantly impacted by thermal radiation. Researchers' attention has recently been drawn to thermal radiation as a mode of energy transfer, and the necessity of including radiative transfer in these processes has been highlighted by recent developments in hypersonic flights, power plants for interplanetary flight, missile re-entry rocket combustion chambers, and gas cooled nuclear reactors. The radiative influence on heat transmission in a vertical porous material was investigated by Raptis [5], Hossain and Takhar [6], Manjula and Muthucumaraswamy [7]. Numerous studies on the effect of radiation on fluid flow have been conducted over the years. Because of very significant contributions to humanity, such as nuclear power plants, studies on the effect of radiation absorption have recently become a trend. Ibrahim et al. [8] conducted one of the early studies on radiation absorption on MHD mixed convective flow for a semi-infinite vertical plate. Sreedevi et al. [9] studied this effect of radiation absorption in the present of hall current for a stretching sheet. We also find the work by Aly et al. [10] who accounted unsteady convective flow with radiation effect for a vertical plate embedded in porous medium, Matta et al. [11] who stressed on the unsteady MHD flow with chemical and radiation effects for a porous plate, also fluid flow past a stretching sheet with heat source and temperature dependent fluid properties was analysed by Hemanta [12]. Khan et al. [13] considered the entropy analysis for hydromagnetic radiative flow of ternary nanofluid by an exponentially stretching surface subject to entropy generation. Some recent studies based on radiative effects are also shown in Refs. [14-18].

The rate of heat generation in the boundary influences the rate of thermal distribution in flow. This is evident in a variety of manufacturing applicati ons, including fire modelling, the fabrication of electro nic chips, etc. Surface temperature and flow velocity both affect how heatwaves spread. As a result, when thermal radiation occurs, a significant difference in temperature is present somewhere in the system.

Because of this, heat generation and absorption for many systems are not constant and rely on the environment and temperature of the system. As found in studies conducted by Nemati et al. [19] who accounted periodic magnetic field effect with heat generation/absorption for a Non-Newtonian fluid, Elsayed et al. [20] presents the effects of heat generation absorption on boundary layer flow of Nano fluid for a stretching cylinder, Khan et al. [21] who examined the variable heat source for unsteady stagnation-point flow of magnetized Oldroyd-B fluid. The impact of ohmic heating for a double diffusive Nano fluid flow for stretching cylinder is considered in the study conducted by Yasir et al. [22]. Also as found in the investigation conducted by Sheikholeslami [23] for thermal solar system, the thermal performance was found to be incremented upon elevating heat absorption.

With the increasing need for advancement, betterment and efficient technology there arises a need for advancement in research approaches and hence making every small progress an important contribution to research and advancement. Due to the temperature and mass differences in a medium there arises a mass and heat flux which are also known as the Soret and Dufour effect respectively, which are important mechanism in the transport phenomenon; it has it varied applications in vapour deposition process for optical fibre fabrication, in fluid flow fractionation, it is used to separate distinct polymers. Okuyade et al. [24] examined the effects of Soret and Dufour for an unsteady convective flow with constant suction. The Dufour effect on unsteady MHD flow past a vertical plate embedded in porous medium with ramped temperature is addressed by Sarma and Ahmed [25]. The Soret effect for a steady MHD fluid flow through a vertical porous plate with aligned magnetic field was presented by Mopuri et al. [26]. We also find in the study of Sowmiya and Kumar [27] who considered the Dufour effect for MHD mixed convective flow with bouyancy effect. Some relevant advancements about Soret and Dufour effects are also highlighted in Refs. [28-32].

The literature review cited above confirms that no attempt has been made to consider the impact of Soret and Dufour under the influence of radiation of absorption, heat source, viscous dissipation, chemical and thermal radiation, with the velocity slip condition for a semi-infinite vertical permeable plate under the presence of pressure gradient. Few researchers even worked on unsteady flow problem with slip effect. Here our main objective is to scrutinize the combined effect of radiation absorption, Soret and Dufour effects with slip paramter for unsteady fluid flow. A comparison has been made with the work presented by Pal and Talukdar [3] and thus the results found in this study are thus verified accordingly. For the purpose of graphical and tabular data, the MATLAB's built-in solver bvp4c technique will be implemented. We prioritise the following research questions in relation to the flow problem under consideration.

What impact does the radiation absorption parameter have on the thermal and solutal boundary layers, fluid momentum, for mixed convective unsteady MHD heat-absorbing fluid flow?

When slip flow is taken into account in the mixed convective flow system for the vertical permeable plate

in presence of MHD and radiation absorption, how are the skin friction, heat, and mass transfer rates are affected?

What changes in the flow field do the Soret and Dufour effects have on the velocity, heat, and mass transfer?

What effects does the time parameter have on the fluid flow over a vertical permeable plate with MHD and slip flow in terms of velocity, heat transfer, and mass transfer?

2. Mathematical Formulation

We address the unsteady two-dimensional mixed convective flow of an incompressible, viscous, electrically conducting, and heat-absorbing fluid through a semi-infinite vertical permeable plate submerged in a uniform porous medium with a slip boundary condition at the interface of the porous and fluid layers.

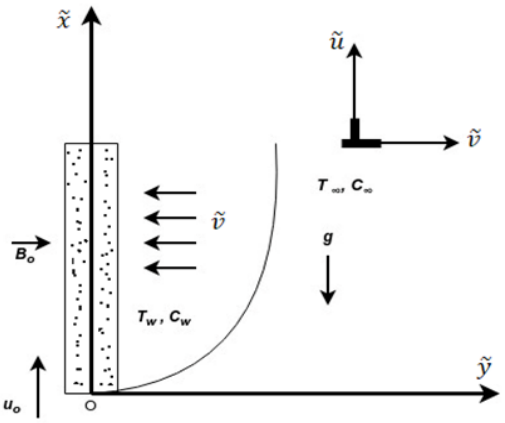

Figure 1. Geometry of the problem

In the presence of radiation and concentration buoyancy effects in the direction of the $\tilde{y}$-axis, a uniform transverse magnetic field of magnitude B_0 is applied. The induced magnetic field and the Hall Effect are thought to be insignificant due to the relatively low transversely applied magnetic field and magnetic Reynolds number. It is presumptively assumed that no voltage is applied, which denotes that there is no electric field. All physical variables are independent of $\tilde{x}$ since the motion is two-dimensional and the length of the plate is sufficient. The temperature and concentration on the wall are kept constant at T_w and C_w, respectively, which are greater than $T_\infty$and $C_\infty$of the ambient fluid. Additionally, it is assumed that the diffusing species and the fluid undergo a homogenous first-order chemical reaction with rate constant $\widetilde{Kr}$.

The governing equations that describe the physical conditions under these hypotheses, in addition to Boussinesq's approximation, are characterized in vector form as: (Ramya et al. [4], Kebede et al. [18], Sarma and Ahmed [25]).

Conservation of Mass

$$\nabla.\boldsymbol{V} = 0 \tag{1}$$

Conservation of Momentum

$$\rho\left[\frac{\partial \boldsymbol{V}}{\partial \tilde{t}} + (\boldsymbol{V}.\nabla)\boldsymbol{V}\right] = -\nabla P + \boldsymbol{J}\times\boldsymbol{B} + \rho g + \mu\nabla^2\boldsymbol{V} - \frac{\mu}{\widetilde{K}}\boldsymbol{V} \tag{2}$$

Conservation of Energy

$$\rho c_p\left[\frac{\partial \tilde{T}}{\partial \tilde{t}} + (\boldsymbol{V}.\nabla)\tilde{T}\right] = k\nabla^2\tilde{T} - \nabla\tilde{q}_r - Q_0\left(\tilde{T} - T_\infty\right) + \mu(\nabla\boldsymbol{V}.\nabla\boldsymbol{V}) + Q_1\left(\tilde{C} - C_\infty\right) + \frac{\rho D_m K_T}{c_s}\nabla^2\tilde{C} \tag{3}$$

Conservation of Species

$$\frac{\partial \tilde{C}}{\partial \tilde{t}} + (\boldsymbol{V}.\nabla)\tilde{C} = D_m\nabla^2\tilde{C} + \frac{D_m K_T}{T_m}\nabla^2\tilde{T} - \widetilde{Kr}(\tilde{C} - C_\infty) \tag{4}$$

We now make the standard boundary-layer approximation, based on a scale analysis, and write the governing equations(Pal and Talukdar [3], Ibrahim et al. [8])

$$\frac{\partial \tilde{v}}{\partial \tilde{y}} = 0 \tag{5}$$

$$\frac{\partial \tilde{u}}{\partial \tilde{t}} + \tilde{v}\frac{\partial \tilde{u}}{\partial \tilde{y}} = -\frac{1}{\rho}\frac{\partial P}{\partial \tilde{x}} + \vartheta\frac{\partial^2\tilde{u}}{\partial \tilde{y}^2} + g\left(\beta_T\left(\tilde{T} - \mathrm{T}_\infty\right) + \beta_C(\tilde{C} - C_\infty)\right) - \left(\frac{\sigma B_0^2}{\rho} + \frac{\vartheta}{\widetilde{K}}\right)\tilde{u} \tag{6}$$

$$\frac{\partial \tilde{T}}{\partial \tilde{t}} + \tilde{v}\frac{\partial \tilde{T}}{\partial \tilde{y}} = \alpha\frac{\partial^2\tilde{T}}{\partial \tilde{y}^2} - \frac{1}{\rho c_p}\frac{\partial \tilde{q}_r}{\partial \tilde{y}} - \frac{Q_0}{\rho c_p}\left(\tilde{T} - \mathrm{T}_\infty\right) + \frac{\mu}{\rho c_p}\left(\frac{\partial \tilde{u}}{\partial \tilde{y}}\right)^2 + \frac{Q_1}{\rho c_p}\left(\tilde{\mathrm{C}} - \mathrm{C}_\infty\right) + \frac{D_m K_T}{c_s c_p}\frac{\partial^2\tilde{C}}{\partial \tilde{y}^2} \tag{7}$$

$$\frac{\partial \tilde{C}}{\partial \tilde{t}} + \tilde{v}\frac{\partial \tilde{C}}{\partial \tilde{y}} = D_m\frac{\partial^2\tilde{C}}{\partial \tilde{y}^2} + \frac{D_m K_T}{T_m}\frac{\partial^2\tilde{T}}{\partial \tilde{y}^2} - \widetilde{Kr}(\tilde{C} - \mathrm{C}_\infty) \tag{8}$$

The radiative heat flux $\tilde{q}_r$ can be represented as follows using the Roseland approximation (Raptis [5]):

$$\frac{\partial \tilde{q}_r}{\partial \tilde{y}} = -4a^*\sigma^*\left(T_\infty^4 - \tilde{T}^4\right) \tag{9}$$

It is considered that the temperature variation within the flow is thought to be minimal enough that $\tilde{T}^4$ can be linearized by using the Taylors series to expand around T_∞ and disregarding terms of higher order. Hence

$$\tilde{T}^4 \cong 4\mathrm{T}_\infty^3\tilde{T} - 3\mathrm{T}_\infty^4 \tag{10}$$

The appropriate boundary conditions for the said fluid problem are: (Pal and Talukdar [3])

$$\begin{aligned} &\tilde{u} = \tilde{h}\frac{\partial\tilde{u}}{\partial\tilde{y}}, \qquad \tilde{T} = T_w + \varepsilon(T_w - T_\infty)e^{\tilde{\omega}\tilde{t}}, \\ &\tilde{C} = C_w + \varepsilon(C_w - C_\infty)e^{\tilde{\omega}\tilde{t}} \qquad at\ \ \tilde{y} = 0 \end{aligned} \tag{11}$$

$$\begin{aligned} &\tilde{u} \to \tilde{u}_\infty = u_0\left(1 + \varepsilon e^{\tilde{\omega}\tilde{t}}\right), \qquad \tilde{T} \to \mathrm{T}_\infty, \\ &\tilde{C} \to \mathrm{C}_\infty, \qquad \text{as } \tilde{y} \to \infty \end{aligned} \tag{12}$$

Suction velocity is either a time-dependent function or a constant, as shown by Eq. (5).

$$\tilde{v} = -v_0\left(1 + \varepsilon A e^{\tilde{\omega}\tilde{t}}\right) \tag{13}$$

Here, suction towards the plate is shown by the negative sign. Outside the boundary layer (Kim [33]) Eq. (6) gives:

$$-\frac{1}{\rho}\frac{dP}{d\tilde{x}} = \frac{d\tilde{u}_\infty}{d\tilde{t}} + \frac{\sigma B_0^2}{\rho}\tilde{u}_\infty + \frac{\vartheta}{\tilde{K}}\tilde{u}_\infty \tag{14}$$

The governing equations and their accompanying boundary conditions must now be converted. The following non-dimensional quantities are displayed in a dimensionless manner.

$$\begin{aligned} &u = \frac{\tilde{u}}{u_0}, u_\infty = \frac{\tilde{u}_\infty}{u_0}, \eta = \frac{v_0}{\vartheta}\tilde{y}, t = \frac{v_0^2}{\vartheta}\tilde{t}\,, \omega = \frac{\vartheta}{v_0^2}\tilde{\omega}, \\ &h = \frac{v_0}{\vartheta}\tilde{h}, \qquad T = \frac{\tilde{T} - T_\infty}{T_w - T_\infty}, \qquad C = \frac{\tilde{C} - C_\infty}{C_w - C_\infty} \end{aligned} \tag{15}$$

Eq. (6) to Eq. (8) can be converted to the dimensionless version using the above dimensionless variables:

$$\begin{aligned} &\frac{\partial u}{\partial t} - (1 + \varepsilon A e^{\omega t})\frac{\partial u}{\partial \eta} = \frac{du_\infty}{dt} + \frac{\partial^2 u}{\partial \eta^2} \\ &\qquad + GrT + GmC + \left(M + \frac{1}{K}\right)(u_\infty - u) \end{aligned} \tag{16}$$

$$\begin{aligned} &\frac{\partial T}{\partial t} - (1 + \varepsilon A e^{\omega t})\frac{\partial T}{\partial \eta} = \frac{1}{\mathrm{Pr}}\frac{\partial^2 T}{\partial y^2} - (Rd + Q)T \\ &\qquad + Ec\left(\frac{\partial u}{\partial \eta}\right)^2 + RC + Du\frac{\partial^2 C}{\partial \eta^2} \end{aligned} \tag{17}$$

$$\frac{\partial C}{\partial t} - (1 + \varepsilon A e^{\omega t})\frac{\partial C}{\partial \eta} = \frac{1}{Sc}\frac{\partial^2 C}{\partial \eta^2} + Sr\frac{\partial^2 T}{\partial \eta^2} - KrC \tag{18}$$

The boundary conditions update as:

$$u = h\frac{\partial u}{\partial \eta}, T = 1 + \varepsilon e^{\omega t}, C = 1 + \varepsilon e^{\omega t}\ at\ \eta = 0 \tag{19}$$

$$u \to u_\infty = 1 + \varepsilon e^{\omega t},\ T \to 0,\ C \to 0,\ \text{as}\ \eta \to \infty \tag{20}$$

3. Method of Solution

It is impossible to solve the partial differential Eq. (16) –Eq. (18) with boundary conditions Eq. (19) and Eq. (20) in closed form. It may, however, be solved if these equations are reduced to a set of dimensionless ordinary differential equations by modelling the u(velocity), T(temperature), and C(concentration) as:

$$u(\eta, t) = f_0(\eta) + \varepsilon e^{\omega t} f_1(\eta) + O(\varepsilon^2) \tag{21}$$

$$T(\eta, t) = T_0(\eta) + \varepsilon e^{\omega t} T_1(\eta) + O(\varepsilon^2) \tag{22}$$

$$C(\eta, t) = C_0(\eta) + \varepsilon e^{\omega t} C_1(\eta) + O(\varepsilon^2) \tag{23}$$

Substitute Eq. (21) - Eq. (23) into Eq. (16) -Eq. (20), equalize the harmonic and non-harmonic components, considering only the first order terms $O(\varepsilon)$ and simplifying to yield the following sets of equations for f_0, T_0, C_0 and f_1, T_1, C_1.

$$\begin{aligned} &f_0'' + f_0' - \left(M + \frac{1}{K}\right)f_0 = \\ &\qquad -\left(GrT_0 + GmC_0 + M + \tfrac{1}{K}\right) \end{aligned} \tag{24}$$

$$\begin{aligned} &f_1'' + f_1' - \left(M + \frac{1}{K} + \omega\right)f_1 = \\ &\qquad -\left(GrT_1 + GmC_1 + M + \tfrac{1}{K} + \omega + Af_0'\right) \end{aligned} \tag{25}$$

$$\begin{aligned} &T_0'' + PrT_0' - Pr(Rd + Q)T_0 = \\ &\qquad -Pr\left(RC_0 + DuC_0'' + Ecf_0'^2\right) \end{aligned} \tag{26}$$

$$\begin{aligned} &T_1'' + PrT_1' - Pr(Rd + Q + \omega)T_1 = \\ &\qquad -Pr(RC_1 + DuC_1'' + AT_0' + 2Ecf_0'f_1') \end{aligned} \tag{27}$$

$$C_0'' + ScC_0' - ScKrC_0 = -ScSrT_0'' \tag{28}$$

$$C_1'' + ScC_1' - Sc(Kr + \omega)C_1 = -Sc(AC_0' + SrT_1'') \tag{29}$$

Here the prime represents regular differentiation with respect to η.

The associated boundary conditions are:

$$\begin{aligned} &f_0 = hf_0', \quad f_1 = hf_1', \quad T_0 = 1, \quad T_1 = 1, \\ &C_0 = 1, \quad C_1 = 1 \quad at\ \eta = 0 \end{aligned} \tag{30}$$

$$\begin{aligned} &f_0 = 1\,, \quad f_1 = 1, \quad T_0 \to 0, \quad T_1 \to 0\,, \\ &C_0 \to 0, \quad C_1 \to 0 \quad \text{as}\ \eta \to \infty \end{aligned} \tag{31}$$

Now using bvp4c, a built-in solver in MATLAB(Shampine et al.[34]) the highly coupled non-

linear ordinary differential Eq. (24) – Eq. (29) along with the boundary condition Eq. (30) and Eq. (31) are solved by setting:

$$f_0 = y_1, \quad f_0' = y_2, \quad f_1 = y_3, \quad f_1' = y_4\,,$$
$$T_0 = y_5, \quad T_0' = y_6, \quad T_1 = y_7, \quad T_1' = y_8\,, \tag{32}$$
$$C_0 = y_9, \quad C_0' = y_{10}, \quad C_1 = y_{11}, \quad C_1' = y_{12}$$

By using the equation Eq. (32) into Eq. (24) to Eq. (29) the following system of first order ordinary differential equations, Eq. (33) –Eq. (38) may be derived, along with boundary conditions equations Eq. (39) and Eq. (40):

$$y_2' = \left(M + \frac{1}{K}\right) y_1 - y_2 - \left(Gry_5 + Gmy_9 + M + \frac{1}{K}\right) \tag{33}$$

$$y_4' = \left(M + \frac{1}{K} + \omega\right) y_3 - y_4 - \left(Gry_7 + Gmy_{11} + M + \frac{1}{K} + \omega + Ay_2\right) \tag{34}$$

$$y_6' = \frac{Pr}{1 - PrDuScSr} \times \{(Rd + Q)y_5 - y_6 - Ry_9 - Ecy_2{}^2 - ScDu(Kry_9 - y_{10})\} \tag{35}$$

$$y_8' = \frac{Pr}{1 - PrDuScSr} \times [(Rd + Q + \omega)y_7 - y_8 - Ry_{11} - Ay_6 - 2Ecy_2y_4 - ScDu\{(Kr + \omega)y_{11} - y_{12} - Ay_{10}\}] \tag{36}$$

$$y_{10}' = Sc\left[Kry_9 - y_{10} - Sr\left[\frac{Pr}{1 - PrDuScSr}\{(Rd + Q)y_5 - y_6 - Ry_9 - Ecy_2{}^2 - ScDu(Kry_9 - y_{10})\}\right]\right] \tag{37}$$

$$y_{12}' = Sc\left[(Kr + \omega)y_{11} - y_{12} - Ay_{10} - Sr\left[\frac{Pr}{1 - PrDuScSr}[(Rd + Q + \omega)y_7 - y_8 - Ry_{11} - Ay_6 - 2Ecy_2y_4 - ScDu\{(Kr + \omega)y_{11} - y_{12} - Ay_{10}\}]\right]\right] \tag{38}$$

Boundary Conditions:

$$y_1 = hy_2\,, \quad y_3 = hy_4\,, \quad y_5 = 1, \quad y_7 = 1, \quad y_9 = 1, \quad y_{11} = 1 \quad at\ \eta = 0 \tag{39}$$

$$y_1 = 1\,, \quad y_3 = 1, \quad y_5 \to 0, \quad y_7 \to 0\,, \quad y_9 \to 0, \quad y_{11} \to 0 \ \text{as}\ \eta \to \infty \tag{40}$$

The most essential measures for the current condition are the skin-friction coefficient C_f, Nusselt number Nu and Sherwood number Sh. (Pal and Talukdar [3])

$$C_f = \frac{\mu\left(\frac{\partial \tilde{u}}{\partial \tilde{y}}\right)_{\tilde{y}=0}}{\rho u_0^2} = \left(\frac{\partial u}{\partial \eta}\right)_{\eta=0} = f_0'(0) + \varepsilon e^{\omega t} f_1'(0) \tag{41}$$

$$Nu = \frac{\vartheta\left(\frac{\partial \tilde{T}}{\partial \tilde{y}}\right)_{\tilde{y}=0}}{v_0(\mathrm{T}_w - \mathrm{T}_\infty)} = \left(\frac{\partial T}{\partial \eta}\right)_{\eta=0} = T_0'(0) + \varepsilon e^{\omega t} T_1'(0) \tag{42}$$

$$Sh = \frac{\vartheta\left(\frac{\partial \tilde{C}}{\partial \tilde{y}}\right)_{\tilde{y}=0}}{v_0(\mathrm{C}_w - \mathrm{C}_\infty)} = \left(\frac{\partial C}{\partial \eta}\right)_{\eta=0} = C_0'(0) + \varepsilon e^{\omega t} C_1'(0) \tag{43}$$

4. Results and Discussion

We plot velocity, temperature, and concentration profiles to determine the physical significance of the problem and display the tabular statistics for C_f, Nu, Sh for distinct values of parameters involved. For the sake of this study, we will use the following default values for computation:

$Gr = 4$; $Gm = 2$; $M = 2$; $K = 5$; $Pr = 0.71$;
$Du = 0.6$; $Sc = 0.6$; $Rd = 2$; $Q = 1$; $R = 2$;
$Ec = 0.01$; $Sr = 1$; $Kr = 1$; $A = 0.5$; $\omega = 1$;
$h = 0.2$; $t = 1$; $\varepsilon = 0.01$;

The present calculated numerical values for the skin-friction coefficient, Nusselt number, and Sherwood number that are shown in Table 1, Table 2 and Table 3 and are in excellent agreement with the computed results of Pal and Talukdar [3] which validates the results and data discussed below.

Figure 2-3 depict the actions of magnetic parameter M and permeability parameter K on velocity within the boundary layer. Because of the Lorentz force that acts as the resistive force due to magnetic field reduces the thickness of the momentum boundary layer. We find that upon incrementing K , the resistive force of the porous medium decreases that aids the fluid to move faster hence incrementing fluid velocity. The result is applicable in reservoir engineering for enhanced oil recovery. Table 4 shows a decay about 8% in C_f inside $2 \leq M \leq 4$, whereas C_f undergoes a growth upto 0.4% within the range $5 \leq K \leq 7$.

Figures 4-5 show the impact of Prandtl number Pr taken as 0.71 (air), 1.00 (electrolytic solution), 7.00 (water), 11.40 (water at 4^0C) on velocity and temperature respectively. As Pr grows, the thickness of the thermal boundary layer decreases, just as a higher value of Pr makes the fluid more viscous and decreases the thickness of the momentum boundary layer; slowing the fluid velocity. Thus, as a result, average temperature and velocity are lower within the boundary layer. This is because fluids with a greater Prandtl number have higher viscosity, which reduces velocity. In addition, fluids with smaller values of Pr are highly conductive. Table 4 shows that for values of Pr within the range $0.71 \leq Pr \leq 3$, C_f undergoes negative growth about 7%, while Nu is drastically reduced about 140% whereas we see a positive growth upto 50% in Sh.

Figure 6-7 show the impact of Eckert number Ec on velocity and temperature. In fluid flow Ec is a quantity that establishes the kinetic energy of a flow's relative relevance in a heat transfer scenario. The expression is simplified to a balance of convection and conduction when $Ec \ll 1$ the terms in the energy expressions represent, making it possible to disregard the effects of pressure fluctuations, dissipation, and body forces on energy balance. As a result, a rise in Ec shows that dissipative heat or additional kinetic energy is being accumulated in the fluid particles as a result of frictional heating, which improves the fluid's total velocity and temperature. It is also evident from Table 4 that C_f and Nu is varied by a growth upto 0.1% and 2.2% respectively while Sh is effected by a decay around 1% within the range $0.01 \leq Ec \leq 0.03$.

Consequently, upon varying values of radiation absorption R, both velocity and temperature appear to be increasing, which is due to the buoyancy force generated by the absorption of radiation parameter that subsequently increases the flow rate and temperature profile as seen in Figures 8-9. Taking in account Table 4 the influence of R on C_f, Nu is noted to differ by a positive growth upto 8% and 59% respectively while Sh to be undergoing a decay around 20% within $2 \leq R \leq 4$.

The temperature response is plotted against Du in Figure 10, and it is revealed that the thermal boundary layer is thickened upon improving Du this is due to the fact that an increase in Du denotes a general increase in the concentration gradient over temperature gradient. The temperature field therefore rises as the concentration gradient increases. Consequently, we observe from Table 4 that Nu is improved around 11%, while Sh reduces around 4% for $0.2 \leq Du \leq 0.6$. The impact of both Sr and Du, as seen in Figure 11, is to increase the fluid flow velocity throughout the boundary layer. However, a distinct velocity overshoot exists near the plate, and thereby the profile falls to attain its boundary condition. We also observe that C_f is improved upto 1.5% and 5.6% for Du and Sr respectively.

The effects of Soret Sr on temperature and concentration are seen in Figures 12-13. As seen in figure the fluid flow temperature and species concentration are found to rise as the Soret effect improves, which is due to mass transfer from lower to greater solute concentration driven by the temperature gradient hence higher Soret effect indicate stronger fluid molecule diffusivity. From Table 4 it is interesting to note that in Nu and Sh both get augmented about 5% and 45% respectively with Sr ranging within $0.5 \leq Sr \leq 1.5$.

Figures 14-15 demonstrate velocity and concentration profiles for varied Schmidt number Sc values of 0.22 (hydrogen), 0.30 (helium), 0.60 (water vapour), and 0.78 (ammonia). The velocity profile lowers because of the heavier diffusing species. It is also worth noting that with lower $Sc(0.22)$ value the peak value (at $\eta = 0.8$) is relatively more far from the plate than the highest value (at $\eta = 0.7$) for larger $Sc(0.78)$, and the concentration distribution was established to fall faster as Sc increased, resulting in the velocity and concentration boundary layers being lowered at the same time. Physically stated, a decrease in molecular diffusion results from an increase in Sc. As a result, the concentration of the species is higher for low Sc values and decrease for high Sc values. Furthermore, as presented in Table 4, as the values of Sc vary from $0.60 \leq Sc \leq 2.62$ it can be stated that C_f, Nu and Sh values undergo decay around 11%, 3% and 181% respectively.

As we increase the values of chemical reaction Kr, we see in Figures 16-18 a rise in the velocity and concentration profile, which finally leads to a simultaneous depletion in the velocity and the concentration boundary layer thickness. On the graph,

upon increasing the value of the chemical reaction Kr has a noticeable impact on the concentration boundary layer. The figure makes it abundantly obvious that the concentration of species that is slightly larger than one at the initial point that gradually falls to satisfy the boundary condition at $\eta \to \infty$. Additionally, it has been shown that incrementing the value of Kr results in a drop in the species concentration in the boundary layer. In addition, we notice a fall in the temperature profile, it is clear because when the Kr increases, the thermal boundary layer loses energy, causing the fluid temperature to drop. Furthermore, from Table 4, as the values of Kr vary from $1 \leq Kr \leq 3$ it can be concluded that C_f, Nu and Sh values are decremented about 7.1%, 7% and 64% respectively.

The effect of slip parameter h on the momentum boundary layer is seen in Figure19. Rising h causes the velocity gradient near the surface to increase, before decrementing to its free stream value. Table 4 also shows that within the range $0.2 \leq h \leq 0.4$, the C_f experiences a decay around 23%.

It is also worth noting that when time t increases, each of these factors have opposing effects on velocity, temperature and concentration as seen in Figures 20-22. The velocity gradually approaches its greatest value near the plate, and then the profile falls till it reaches the bare minimum at $\eta \to \infty$. All times are relevant to this circumstance. It is also noticed that the peak value grows with time. In the flow area, temperature rises with passing time. This occurs as a result of the fluid capacity to store heat energy as time goes on. The solutal boundary layer species concentration rises with time, increasing the layer thickness in the process.

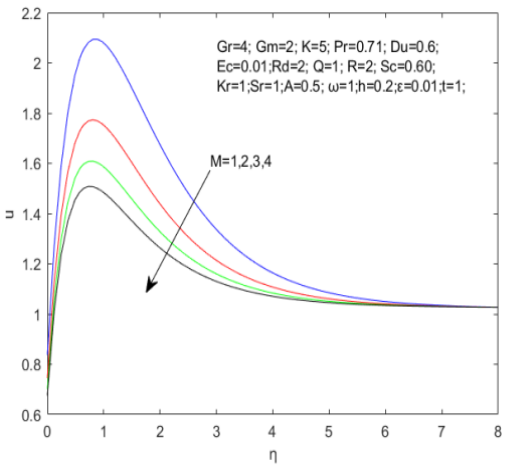

Figure 2. Velocity for varying Magnetic parameter *M*

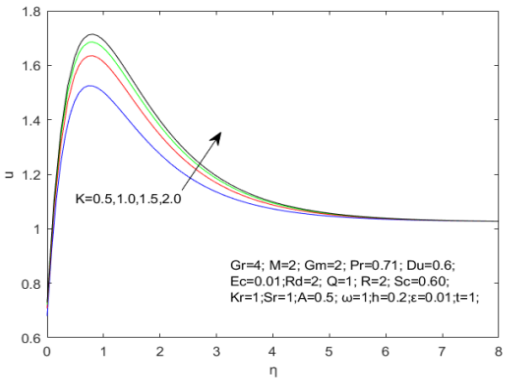

Figure 3. Velocity for varying Permeability parameter K

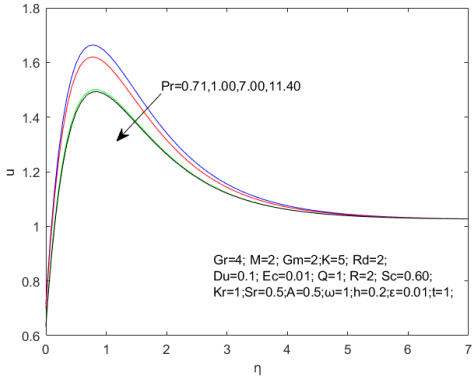

Figure 4. Velocity for varying Prandtl number Pr

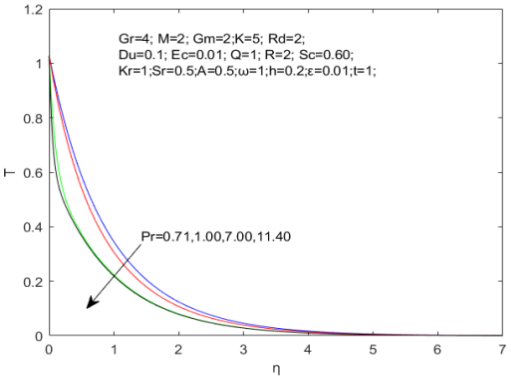

Figure 5. Temperature for varying Prandtl number Pr

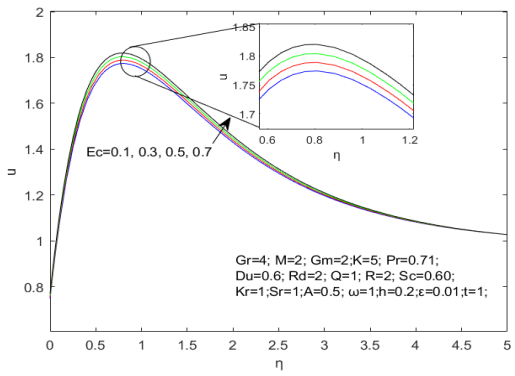

Figure 6. Velocity for varying Eckert number Ec

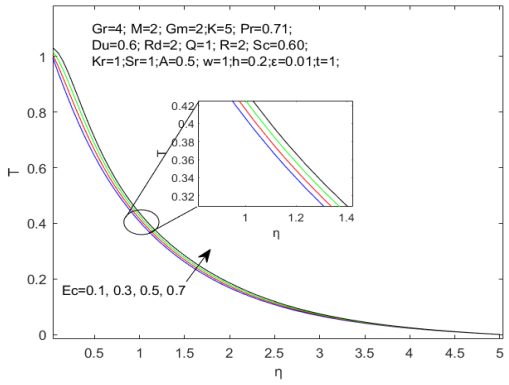

Figure 7. Temperature for varying Eckert number Ec

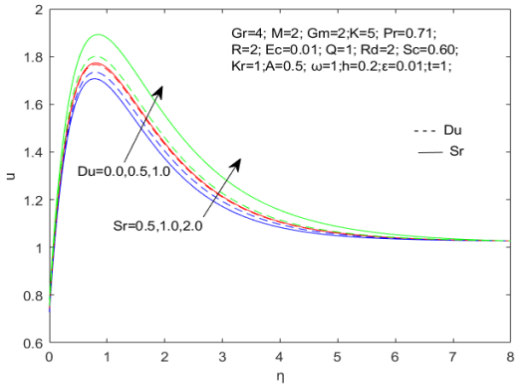

Figure 11. Velocity for varying Soret Sr and Dufour number Du

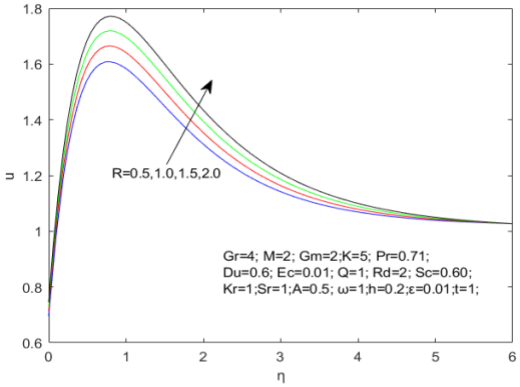

Figure 8. Velocity for varying absorption of radiation parameter R

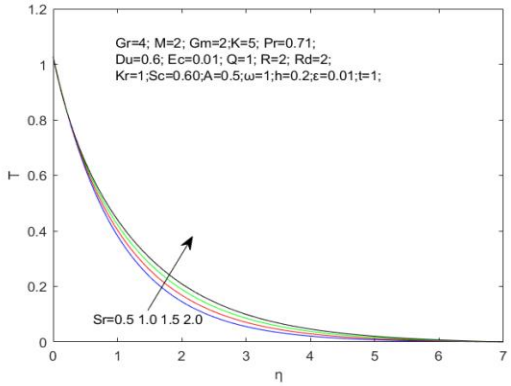

Figure 12. Temperature for varying Soret number Sr

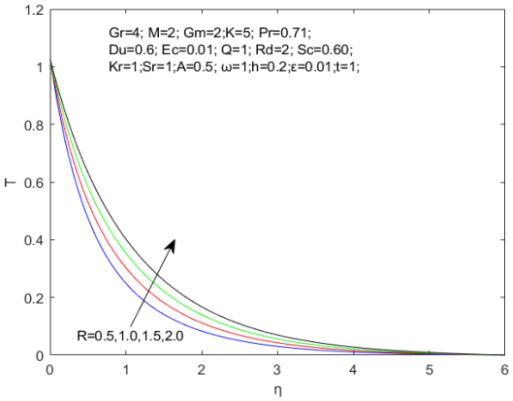

Figure 9. Temperature for varying absorption of radiation parameter R

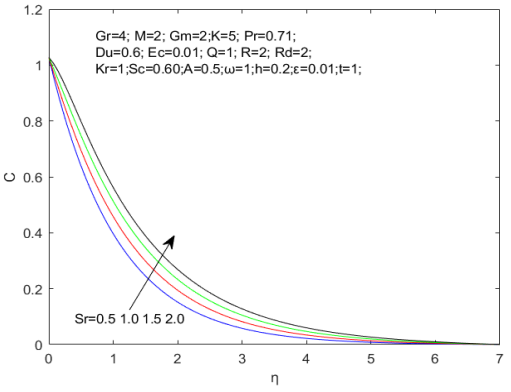

Figure 13. Concentration for varying Soret number Sr

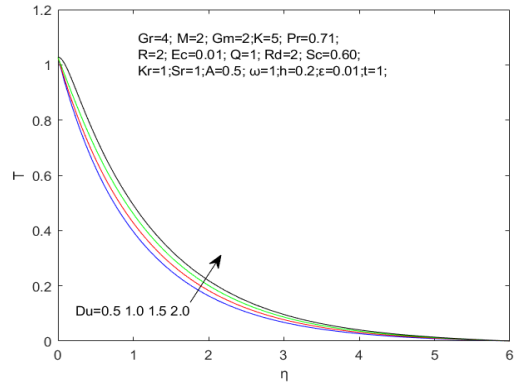

Figure 10. Temperature for varying Dufour Du

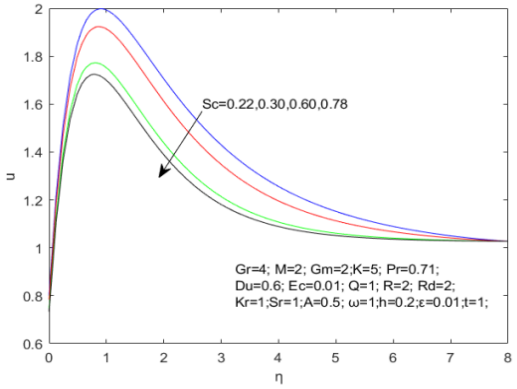

Figure 14. Velocity for varying Schmidt number Sc

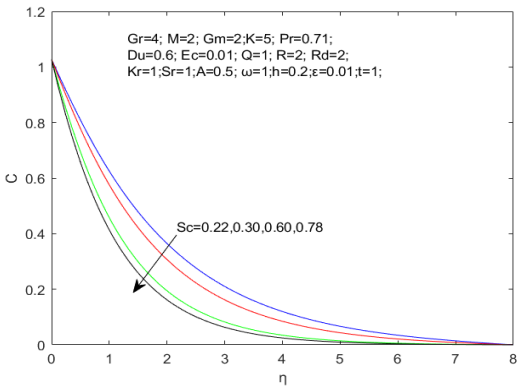

Figure 15. Concentration for varying Schmidt number Sc

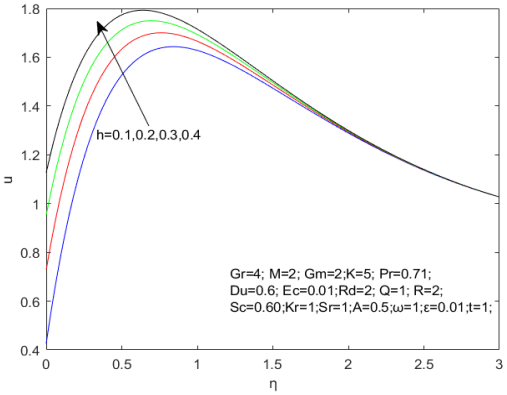

Figure 19. Velocity for varying slip parameter h

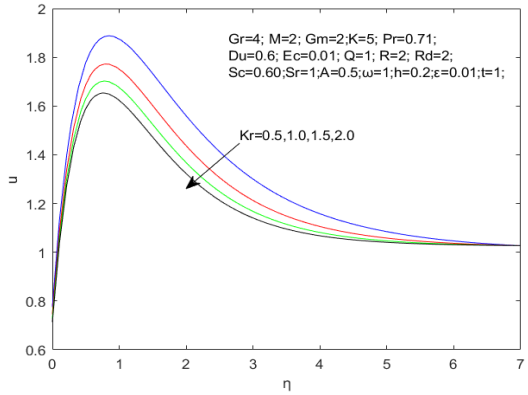

Figure 16. Velocity for varying Chemical reaction Kr

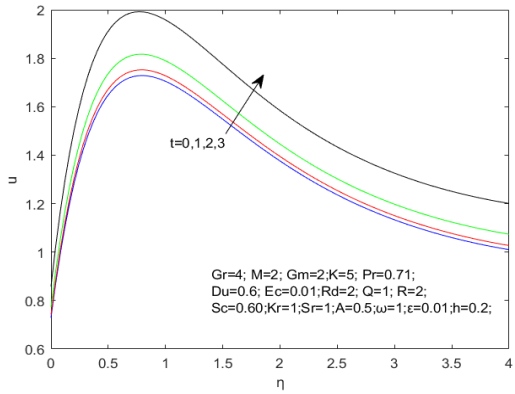

Figure 20. Velocity for varying time t

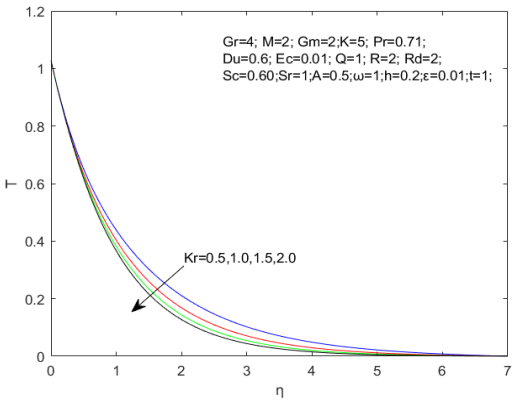

Figure 17. Temperature for varying Chemical reaction Kr

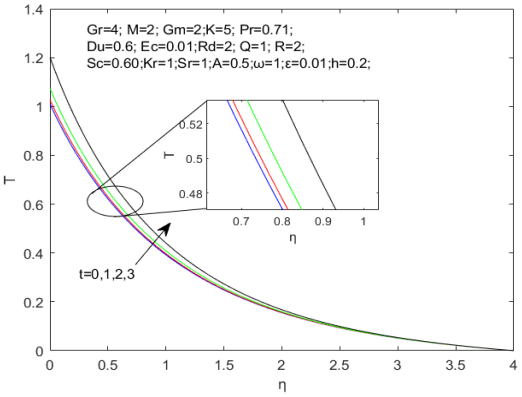

Figure 21. Temperature for varying time t

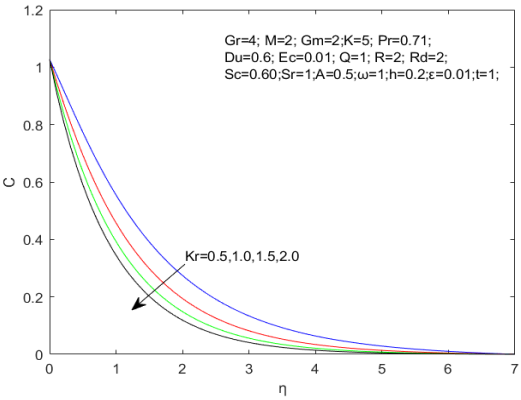

Figure 18. Concentration for varying Chemical reaction Kr

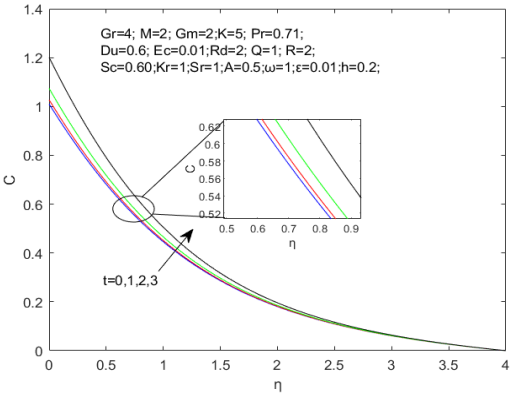

Figure 22. Concentration for varying time t

Table 1. Effects of h on C_f, Nu, Sh for reference values $Pr = 0.7, A = 0.5, \varepsilon = 0.2, \omega = 0.1,$ $t = 1.0, Kr = 0.1, Du = 0.0, Ec = 0.0, Sr = 0.0$

h	Pal and Talukdar [3]			Present		
	C_f	Nu	Sh	C_f	Nu	Sh
0.0	6.4047	-1.3822	-0.9087	6.4047	-1.3822	-0.9088
0.1	5.3082	-1.3822	-0.9087	5.3082	-1.3822	-0.9088
0.3	3.9540	-1.3822	-0.9087	3.9540	-1.3822	-0.9088
0.5	3.1503	-1.3822	-0.9087	3.1503	-1.3822	-0.9088

Table 2. Effects of Rd on C_f, Nu, Sh for reference values $Pr = 0.7, A = 0.5, \varepsilon = 0.2, \omega = 0.1,$ $t = 1.0, h = 0.3, \quad Kr = 0.1, Du = 0.0, Ec = 0.0, Sr = 0.0$

Rd	Pal and Talukdar [3]			Present		
	C_f	Nu	Sh	C_f	Nu	Sh
1.0	4.1838	-0.9254	-0.9087	4.1838	-0.9255	-0.9088
2.0	3.9540	-1.3822	-0.9087	3.9540	-1.3822	-0.9088
3.0	3.8015	-1.7436	-0.9087	3.8015	-1.7437	-0.9088
4.0	3.6901	-2.0488	-0.9087	3.6901	-2.0489	-0.9088

Table 3. Effects of Kr onC_f, Nu, Sh for reference values $Pr = 0.7, A = 0.5, \varepsilon = 0.2, \omega = 0.1,$ $t = 1.0, h = 0.3, \quad Du = 0.0, Ec = 0.0, Sr = 0.0$

Kr	Pal and Talukdar [3]			Present		
	C_f	Nu	Sh	C_f	Nu	Sh
0.00	4.0441	-1.3400	-0.8098	4.0439	-1.3401	-0.8099
0.50	3.7512	-1.4825	-1.1864	3.7513	-1.4825	-1.1864
0.75	3.6744	-1.5226	-1.3178	3.6744	-1.5227	-1.3178
1.00	3.6149	-1.5546	-1.4325	3.6149	-1.5546	-1.4326

Table 4: Effects of $Gr, Gm, M, K, Pr, R, Q, Rd, Ec, Du, Sc, Sr, Kr, h$ onC_f, Nu, Sh for reference values $A = 0.5; \omega = 1; h = 0.2; t = 1; \ \varepsilon = 0.01$

Gr	Gm	M	K	Pr	R	Q	Rd	Ec	Du	Sc	Sr	Kr	h	C_f	Nu	Sh
4	2	2	5	0.71	2	1	2	0.01	0.2	0.60	0.5	1	0.2	3.5876	-1.1492	-0.9396
5														3.9266	-1.1470	-0.9402
6														4.2658	-1.1446	-0.9410
	3													3.9499	-1.1468	-0.9403
	4													4.3123	-1.1441	-0.9411
		3												3.4028	-1.1511	-0.9390

4												3.2975	-1.1523	-0.9387
	6											3.5961	-1.1492	-0.9396
	7											3.6022	-1.1491	-0.9396
		1										3.5158	-1.3737	-0.8760
		3										3.3234	-2.7564	-0.4704
			3									3.7331	-0.8057	-1.0347
			4									3.8726	-0.4742	-1.1264
				2								3.4746	-1.4491	-0.8557
				3								3.3902	-1.7060	-0.7830
					3							3.4746	-1.4491	-0.8557
					4							3.3902	-1.7060	-0.7830
						0.02						3.5891	-1.1367	-0.9433
						0.03						3.5906	-1.1241	-0.9470
							0.4					3.6139	-1.0892	-0.9651
							0.6					3.6407	-1.0246	-0.9740
								1				3.4272	-1.2000	-1.2911
								2.62				3.2959	-1.2194	-1.7998
									1			3.6922	-1.1160	-0.7195
									1.5			3.7875	-1.0870	-0.5106
										2		3.4277	-1.2010	-1.2773
										3		3.3332	-1.2262	-1.5412
											0.3	3.1279	-1.1526	-0.9386
											0.4	2.7726	-1.1548	-0.9380

Conclusion

The following interpretations of the flow field may be formed for varying values of parameters associated in the flow field:

1. Fluids with a high Prandtl number have a high viscosity and thermal conductivity, which deteriorate the skin friction about 7% and heat transfer rate about 140% but improves the mass transfer rate upto 50% when Pr changes from 0.71 to 3.0
2. As the radiation absorption parameter improves the skin friction improves about 8% and heat flow rate significantly augments around 59%, while Sherwood number reduces around 20% when R alters from 2 to 4
3. The viscous dissipation created in the fluid flow tends to increase velocity, temperature distribution and improves the heat flow rate about 2.2% for when Ec varying from 0.01 to 0.03
4. The Soret effect has been found to significantly improve the skin friction, heat and mass transfer rates by significant percentages of about 5.6%, 5% and 45% respectively when Sr changes from 0.5 to 1.5.
5. The Dufour effect can be improved to augment the heat transfer rate about 11% and cause mass transfer rate to deteriorate around 4% when Du shifts from 0.2 to 0.6.
6. The slip parameter can be improved to enhance velocity profile and to deteriorate skin friction around 2.3% as h shifts from 0.2 to 0.4.

7. The velocity, temperature, and species concentration distribution all continue growing as more time goes by.

It is intended that the physics of flow across the permeable vertical plate with velocity slip may be used as the foundation for various engineering and scientific applications using our current model. Additionally, it can serve as inspiration for next experiments, which are now lacking.

In subsequent studies, we will use the proper velocity slip notion to further generalize comparisons to various body forms.

Nomenclature

a^* Mean absorption coefficient

A Real positive constant

$\boldsymbol{B}$ Magnetic field flux

B_0 Magnetic field strength T

$\tilde{C}$ Species concentration Kgm^{-3}

C A scaled concentration

C_f Skin friction

C_∞ Ambient fluid's species concentration Kgm^{-3}

C_w Wall concentration

c_p Specific heat at constant pressure $JKg^{-1}K^{-1}$

c_s Concentration susceptibility

D_m Molecular diffusivity coefficient m^2s^{-1}

Du Dufour number $\frac{D_m K_T}{c_s c_p \vartheta}\left(\frac{\mathrm{C}_w-\mathrm{C}_\infty}{\mathrm{T}_w-\mathrm{T}_\infty}\right)$

Ec Eckert number $\frac{u_0^2}{c_p(\mathrm{T}_w-\mathrm{T}_\infty)}$

Gm Solutal Grashof number $\frac{g\beta_C(\mathrm{C}_w-\mathrm{C}_\infty)\vartheta}{v_0^2 u_0}$

Gr Thermal Grashof number $\frac{\mathrm{g}\beta_T(\mathrm{T}_w-\mathrm{T}_\infty)\vartheta}{v_0^2 u_0}$

g Acceleration due to gravity ms^{-2}

$\tilde{h}$ Dimensional slip parameter m

h Non-dimensional slip parameter

$\boldsymbol{J}$ Current density

k thermal conductivity $Jm^{-1}s^{-1}K^{-1}$

$\tilde{K}$ Permeability of porous medium m^2

K Non-dimensional permeability $\frac{v_0^2\tilde{K}}{\vartheta^2}$

$\widetilde{Kr}$ Dimensional chemical reaction

Kr Non-dimensional chemical reaction $\frac{\widetilde{Kr}\vartheta}{v_0^2}$

K_T Thermal diffusion ratio Kgm^{-3}

M Magnetic parameter $\frac{\sigma B_0^2\vartheta}{\rho v_0^2}$

Nu Nusselt number

P Fluid pressure Nm^{-2}

Pr Prandtl number $\frac{\vartheta}{\alpha}$

Q Non-dimensional heat source parameter $\frac{Q_0\vartheta}{\rho c_p v_0^2}$

Q_0 Dimensional heat absorption coefficient $\mathrm{W}m^{-3}$

Q_1 Dimensional radiation of absorption

$\tilde{q}_r$ Radiative heat flux Wm^{-2}

R Non-dimensional radiation of absorption $\frac{(\mathrm{C}_w-\mathrm{C}_\infty)\vartheta}{(\mathrm{T}_w-\mathrm{T}_\infty)v_0^2}$

Rd Radiation parameter $\frac{16a^*\sigma^* T_\infty^3\vartheta}{\rho c_p v_0^2}$

Sc Schmidt number $\frac{\vartheta}{D_m}$

Sh Sherwood number

Sr Soret number $\frac{D_m K_T}{\vartheta T_m}\left(\frac{\mathrm{T}_w-\mathrm{T}_\infty}{\mathrm{C}_w-\mathrm{C}_\infty}\right)$

$\tilde{T}$ Dimensional fluid temperature K

T A scaled temperature

T_∞ Ambient fluid temperature K

T_m Mean fluid temperature

$\tilde{t}$ Dimensional time s

t Non-dimensional time

u A scaled velocity

$\tilde{u}$ Dimensional velocities x̃ direction ms^{-1}

u_0 Characteristic velocity ms^{-1}

u_∞ Non- dimensional free stream

$\tilde{u}_\infty$ Dimensional free stream velocity ms^{-1}

$\tilde{v}$ Dimensional velocities ỹ direction ms^{-1}

v_0 Scale of suction velocity ms^{-1}

$\boldsymbol{V}$ Flow velocity vector

$\tilde{x}$ Dimensional distances along the plate m

$\tilde{y}$ Dimensional distances perpendicular to the plate m

Greek symbols

β_C Concentration expansion coefficients Kg^{-1}

β_T Thermal expansion coefficients K^{-1}

α Fluid thermal diffusivity $m^2\mathrm{s}^{-1}$

ρ Fluid density $\mathrm{Kg}m^{-3}$

σ Electrical conductivity of fluid $\mathrm{Kg}^{-1}m^{-3}s^3A^2$

ϑ Kinematic viscosity m^2s^{-1}

μ Dynamic viscosity $Kgm^{-1}s^{-1}$

η A scaled coordinate m

σ^* Stefan-Boltzmann constant $Wm^{-2}K^{-4}$

ε A small positive constant

$\widetilde{\omega}$ Frequency of oscillation s^{-1}

ω A scaled frequency

∇ Differential operator

References

[1] S. Goldstein, 1965. *Modern developments in fluid dynamics*. New York, Dover Publications, 1965.

[2] B. G. S and Joseph D D, 1967. Boundary conditions at a natural permeable wall, *Journal of Fluid Mechanics*, 30(1), pp. 197–207

[3] D. Pal and B. Talukdar, 2010. Perturbation analysis of unsteady magnetohydrodynamic convective heat and mass transfer in a boundary layer slip flow past a vertical permeable plate with thermal radiation and chemical reaction, *Communications in Nonlinear Science and Numerical Simulation*, 15(7), pp. 1813–1830 doi: 10.1016/j.cnsns.2009.07.011.

[4] D. Ramya, R. S. Raju, J. A. Rao, and A. J. Chamkha, 2018. Effects of velocity and thermal wall slip on magnetohydrodynamics (MHD) boundary layer viscous flow and heat transfer of a Nano fluid over a non-linearly-stretching sheet : a numerical study, *Propulsion and Power Research*, 7(2), pp. 182–195 doi: 10.1016/j.jppr.2018.04.003.

[5] A. Raptis, 2011. Free convective oscillatory flow and mass transfer past a porous plate in the presence of radiation for an optically thin fluid, *Thermal Science*, 15(3), pp. 849–857 doi: 10.2298/TSCI101208032R.

[6] M. A. Hossain and H. S. Takhar, 1996.Radiation effect on mixed convection along a vertical plate with uniform surface temperature, *Heat and Mass Transfer*, 31(4), pp. 243–248 doi: 10.1007/s002310050052.

[7] L. Manjula and R. Muthucumaraswamy, 2021. Heat and Mass Transfer Effect on an Infinite Vertical Plate in the Presence of Hall Current and Thermal Radiation with Variable Temperature, *International Journal of Applied Mechanics and Engineering*, 26(3), pp. 131–140 doi: 10.2478/ijame-2021-0040.

[8] F. S. Ibrahim, A. M. Elaiw, and A. A. Bakr, 2008. Effect of the chemical reaction and radiation absorption on the unsteady MHD free convection flow past a semi infinite vertical permeable moving plate with heat source and suction, *Communications in Nonlinear Science and Numerical Simulation*, 13(6), pp. 1056–1066 doi: 10.1016/j.cnsns.2006.09.007.

[9] G. Sreedevi, R. R. Rao, D. R. V. P. Rao, and A. J. Chamkha, 2016. Combined influence of radiation absorption and Hall current effects on MHD double-diffusive free convective flow past a stretching sheet, *Ain Shams Engineering Journal*, 7(1), pp. 383–397 doi: 10.1016/j.asej.2015.11.024.

[10] A. M. Aly, A. J. Chamkha, and Z. A. S. Raizah, 2020. Unsteady coupled heat and mass transfer by free convection from a vertical plate embedded in porous media under impacts of radiation and chemical reaction, *Journal of Heat and Mass Transfer Research*, 7(2), pp. 95–103 doi: 10.22075/JHMTR.2019.10763.1149.

[11] S. Matta, B. S. Malga, L. Appidi, and P. P. Kumar, 2021. Radiation and chemical reaction effects on unsteady MHD free convention mass transfer fluid flow in a porous plate, *Indian Journal of Science and Technology*, 14(8), pp. 707–717 doi: 10.17485/ijst/v14i8.20.

[12] H. Konwar, 2022. Flow , Heat and Mass Transfer past a Stretching Sheet with Temperature Dependent Fluid Properties in Porous Medium, *Journal of Heat and Mass Transfer Research*,9, pp. 17–26 doi: 10.22075/jhmtr.2022.25036.1357.

[13] S. A. Khan, T. Hayat, and A. Alsaedi, 2022. Thermal conductivity performance for ternary hybrid nanomaterial subject to entropy generation, *Energy Reports*, 8, pp. 9997–10005 doi: 10.1016/j.egyr.2022.07.149.

[14] S. A. Khan, T. Hayat, A. Alsaedi, and B. Ahmad, 2021. Melting heat transportation in radiative flow of nanomaterials with irreversibility analysis, *Renewable and Sustainable Energy Reviews*, 140, pp. 110739 doi: https://doi.org/10.1016/j.rser.2021.110739.

[15] M. Yasir, M. Khan, and A. Ahmed, 2022. Non-linear radiative flow of unsteady Oldroyd-B nanofluid subject to Arrhenius activation energy, *Waves in Random and Complex Media*, 0(0), pp. 1–15 doi: 10.1080/17455030.2022.2135791.

[16] S. A. Khan, T. Hayat, and A. Alsaedi, 2022. Entropy optimization for nanofluid flow with radiation subject to a porous medium, *Journal of Petroleum Science and Engineering*, 217, pp. 110864 doi: https://doi.org/10.1016/j.petrol.2022.110864.

[17] S. A. Khan, T. Hayat, and A. Alsaedi, 2022. Numerical study for entropy optimized radiative unsteady flow of Prandtl liquid, *Fuel, 319, pp*. 123601 doi: https://doi.org/10.1016/j.fuel.2022.123601.

[18] T. Kebede, E. Haile, G. Awgichew, and T. Walelign, 2020. Heat and Mass Transfer in Unsteady Boundary Layer Flow of Williamson Nanofluids, *Journal of Applied Mathematics*, 2020(1890972) doi: https://doi.org/10.1155/2020/1890972.

[19] M. Nemati, M. Sefid, and A. R. Rahmati, 2021. Analysis of the Effect of Periodic Magnetic Field, Heat Absorption / Generation and Aspect Ratio of the Enclosure on Non-Newtonian Natural Convection, *Journal of Heat and Mass Transfer Research*,8, pp. 187–203 doi: 10.22075/JHMTR.2021.22119.1322.

[20] E. M. A. Elbashbeshy, H. G. Asker, and B. Nagy, 2022. The effects of heat generation absorption on boundary layer flow of a nanofluid containing gyrotactic microorganisms over an inclined stretching

cylinder, *Ain Shams Engineering Journal*, 13(5), pp. 101690 doi: 10.1016/j.asej.2022.101690.

[21] M. Khan, M. Yasir, A. Saleh, S. Sivasankaran, Y. Rajeh, and A. Ahmed, 2022. Variable heat source in stagnation-point unsteady flow of magnetized Oldroyd-B fluid with cubic autocatalysis chemical reaction, Ain *Shams Engineering Journal*, 13(3), pp. 101610 doi: 10.1016/j.asej.2021.10.005.

[22] M. Yasir, A. Ahmed, M. Khan, Z. Iqbal, and M. Azam, 2022. Impact of ohmic heating on energy transport in double diffusive Oldroyd-B nanofluid flow induced by stretchable cylindrical surface, *Proceedings of the Institution of Mechanical Engineers, Part E: Journal of Process Mechanical Engineering*, 0(0) doi: 10.1177/09544089211064116.

[23] M. Sheikholeslami, 2022. Numerical investigation of solar system equipped with innovative turbulator and hybrid nanofluid, *Solar Energy Materials and Solar Cells*, 243, pp. 111786

[24] W. I. A. Okuyade, T. M. Abbey, and A. T. Gima-laabel, 2018. Unsteady MHD free convective chemically reacting fluid flow over a vertical plate with thermal radiation, Dufour, Soret and constant suction effects, *Alexandria Engineering Journal*, 57(4), pp. 3863–3871 doi: 10.1016/j.aej.2018.02.006.

[25] S. Sarma and N. Ahmed, 2022. *Dufour effect on unsteady MHD flow past a vertical plate embedded in porous medium with ramped temperature*. Nature Publishing Group UK, 2022. Doi: 10.1038/s41598-022-15603-x.

[26] O. Mopuri, R. Kodi, C. Ganteda, R. Srikakulapu, and G. Lorenzini, 2022. MHD Heat and Mass Transfer Steady Flow of a Convective Fluid Through a Porous Plate in The Presence of Diffusion Thermo and Aligned Magnetic Field, *Journal of Advanced Research in Fluid Mechanics and Thermal Sciences*,89(1), pp. 62–76 doi: 10.37934/arfmts.89.1.6276.

[27] C. Sowmiya and B. R. Kumar, 2022. MHD mixed convection flow in a permeable vertical plate with buoyancy and Dufour effects, *Journal of Porous Media*, 25(11), pp. 71–81 doi: 10.1615/JPorMedia.2022044034.

[28] M. Venkateswarlu, D. V. Lakshmi, and O. D. Makinde, 2020. Thermodynamic analysis of hall current and Soret number effect on hydromagnetic Couette flow in a rotating system with a convective boundary condition, *Heat Transfer Research*, 51(1), pp. 83–102 doi: 10.1615/HeatTransRes.2019027139.

[29] V. Meenakshi, 2021. Dufour and Soret Effect on Unsteady MHD Free Convection and Mass Transfer Flow Past an Impulsively Started Vertical Porous Plate Considering with Heat Generation, *Journal of Heat and Mass Transfer Research*, 8(2), pp. 257–266 doi: 10.22075/JHMTR.2021.21229.1301.

[30] B. K. Taid and N. Ahmed, 2022. MHD Free Convection Flow across an Inclined Porous Plate in the Presence of Heat Source, Soret Effect, and Chemical Reaction Affected by Viscous Dissipation Ohmic Heating, *Biointerface Research in Applied Chemistry*, 12(5), pp. 6280–6296 doi: https://doi.org/10.33263/BRIAC125.628 06296.

[31] M. Yasir, M. Khan, and Z. U. Malik, 2023. Analysis of thermophoretic particle deposition with Soret-Dufour in a flow of fluid exhibit relaxation/retardation times effect, *International Communications in Heat and Mass Transfer*, 141, pp. 106577 doi: https://doi.org/10.1016/j.icheatmasstransfer .2022.106577.

[32] S. A. Khan, T. Hayat, and A. Alsaedi, 2022. Simultaneous features of Soret and Dufour in entropy optimized flow of reiner-rivlin fluid considering thermal radiation, *International Communications in Heat and Mass Transfer*, 137, pp. 106297 doi: https://doi.org/10.1016/j.icheatmasstra nsfer.2022.106297.

[33] Y. J. Kim, 2000. Unsteady MHD convective heat transfer past a semi-infinite vertical porous moving plate with variable suction, *International Journal of Engineering Science*, 38(8), pp. 833–845 doi: 10.1016/S0020-7225(99)00063-4.

[34] L. Shampine, J. Kierzenka, and M. Reichelt, 2000. Solving boundary value problems for ordinary differential equations in MATLAB with bvp4c, *Tutorial Notes*, 75275, pp. 1–27 doi: https://classes.engineering.wustl.edu/ch e512/bvp_paper.pdf.